Designing Active Mode Double Air Pass Solar Tunnel Dryer and Analysis of Factors Affecting Energy and Exergy Outcome Performance of the Drying System

Dagim Kebede Gari and A. Venkata Ramayya*
Departement of Sustainable Energyl Engineering, Jimma Institute of Technology, Jimma University, Jimma, Ethiopia,
*Corresponding author: ganikavenkata@gmail.com

ABSTARCT
This study aims to design and performance evaluation of an active mode solar tunnel dryer with a double air pass for drying charcoal dust briquette. The influence of solar tunnel dryer shape, heat flux input, and air velocity on outlet air temperature, energy, and exergy parameters was studied by developing a mathematical model. The numerical solution was programmed in PYTHON software. Three shapes of solar tunnel dryers are designed with similar collector surface areas: Quonset, triangular and rectangular. The outlet temperature, thermal efficiency, and exergy efficiency vary from 41.4℃to 73.85℃, 79.2% to 86.5%, and 55% to 79.7%, respectively, for heat flux input variation between 194 W/m^2 and 1052 W/m^2 at 1 m/s and semi-circular shape dryer. The effect of the solar tunnel dryer shape was performed. The higher outlet temperature, energy, and exergy value was found for a semi-circular shape, followed by a triangular shape. The most negligible value was found for a rectangular shape. The analysis of air velocity variation reveals that the value of energy efficiency and exergy efficiency increases, and the value of outlet temperature decreases as air velocity increases. Therefore, the energy and exergy performance of active mode double air pass solar tunnel dryer is affected by solar tunnel dryer shape, input heat flux, and air stream velocity.

Keywords: Air Velocity, Energy, Exergy, Heat Flux Input, Outlet temperature, Solar Tunnel Dryer Shape

INTRODUCTION

Several Sub-Saharan African countries have been experiencing energy crises because of the potential growth of convectional charcoal demand, and 80% to 90 % of urban households depend on the unsustainable source of charcoal for cooking and heating (Arisaka, 2019; Mwampamba et al., 2013; Ngusale et al., 2014). In response to the energy crisis, the uptake of biomass briquettes ensures sustainable energy and environment, enhances efficient and effective use, and promotes great access to an appropriate, alternative source of biomass energy (Guoa et al., 2020). Biomass briquette is a military mixture of immiscible solid and fluid constituents considered porous media, making the drying process a more complex phenomenon (Kolesnikov et al., 2020). But, the majority of SSA country producers use an open sun drying (OSD) technique that leads to vital challenges (Ngusale et al., 2014). Thus, the adoption of biomass briquettes is very low because of drying space scarcity and difficulties with drying, which were the major challenges for the producers.

The drying process is a mass and heat transfer phenomenon that removes moisture from a solid product by passing hot air around it to carry away the released vapor. Solar drying technology has been used to dry plants, seeds, fruits, meat, fish, wood, and other agricultural and forest products since the early stage of mankind to benefit from the free and renewable energy source provided by the sun (Salvatierra-Rojas et al., 2021). Drying technology was developed to mitigate the challenges of OSD techniques depending on conventional and renewable energy sources. The major drawback of drying systems operating with convectional energy attracts researchers toward renewable energy sources, especially focusing on solar radiation. A few kinds of research have been done on the study of biomass briquette drying behavior, factors that affect evaporation rate, and the design of appropriate solar drying systems.

Accordingly, this work intended to design an active mode double air pass solar tunnel dryer for drying charcoal dust briquette and to study the influence of STD shape, input heat flux, and air stream velocity variation on the performance by considering the double air pass solar tunnel dryer with no load. The optimum design was selected through a comparative analysis of factors affecting the solar drying system. The performance was computed analytically by developing a mathematical model based on the mass, energy, and exergy balance principle of thermodynamics to determine the outlet air temperature, the useful energy and exergy output, and thermal and exergy efficiency. Finally, the result of the analytical analysis was validated by comparing it with related research studies.

MATERIALS AND METHODS

The proposed drying system was studied for a test site at Jimma University Institute of Technology in Jimma zone, Ethiopia ($7° 40'0''N, 36° 50'0''E$), about 346 km from Addis Ababa in South West. The effect of ambient parameters on the drying system will be investigated based on the ambient solar radiation, temperature, wind speed, relative humidity, and specific humidity of Jimma zone, Ethiopia. The air temperature at the inlet, the shape of the drying system, input heat flux, and air stream velocity in both heating and drying chambers were taken as independent variables. Therefore, the hourly solar radiation of the proposed location was used as the input heat flux that varies from $6:00$ up to $17:00$ (for 11 hours) to examine its effect. The influence of air stream velocity on the dryer performance was evaluated for 0.8923, and $4\ m/s$per heat flux inputs. A constant air velocity was considered throughout the drying system, and the corresponding variation of air stream flow rate inside the heating and drying chamber at a constant area is listed in Table 1.

Table 1: Variation of Air Flow Rate at Different Velocity Conditions

Air Velocity (m/s)	Heating Chamber		Drying Chamber	
	Mass Flow Rate of Air (Kg/s)	Volumetric Flow Rate of Air (m^3/s)	Mass Flow Rate of Air (Kg/s)	Volumetric Flow Rate of Air (m^3/s)
1	0.0181	0.01477	0.0352	0.02872
2	0.0362	0.02955	0.0704	0.05744
3	0.0543	0.04432	0.1055	0.08615
4	0.0724	0.05909	0.1407	0.11487

The influence of solar tunnel dryer shape was studied by developing Semi-circular (Quonset), Rectangular, and Triangular shape solar tunnel dryers, as shown in Figure 1, and the cross-sectional view is presented in Figure 2. Comparative analysis was done to select the dryer with better performance.

Description of Drying System

The design and performance analysis of the double air passes solar tunnel dryer for biomass-derived charcoal dust briquette was conducted based on the schematic diagram shown in Figure 2. The main components of the dryer are cover, absorber plate, drying bed, bottom floor, frame structure, overall support structure, fans, and PV panel. A single layer of a UV-stabilized semi-transparent polyethylene sheet of $0.2\ mm$ thickness cover ***was*** placed over the heating chamber. A black-painted aluminum sheet of $0.4\ mm$thick absorber plate was used to utilize solar radiation and concomitantly heat the air stream inside the heating and drying chamber. The bottom floor and edges of the drying chamber are made from $5\ mm$ thick wood timber to reduce backside heat loss and to support the charcoal briquette with a drying

bed. An aluminum plate and duct were selected to construct the frame structure and drying bed. The concrete material was considered an overall support structure to carry the weight of the drying system. The design dimension is listed in Table 2.

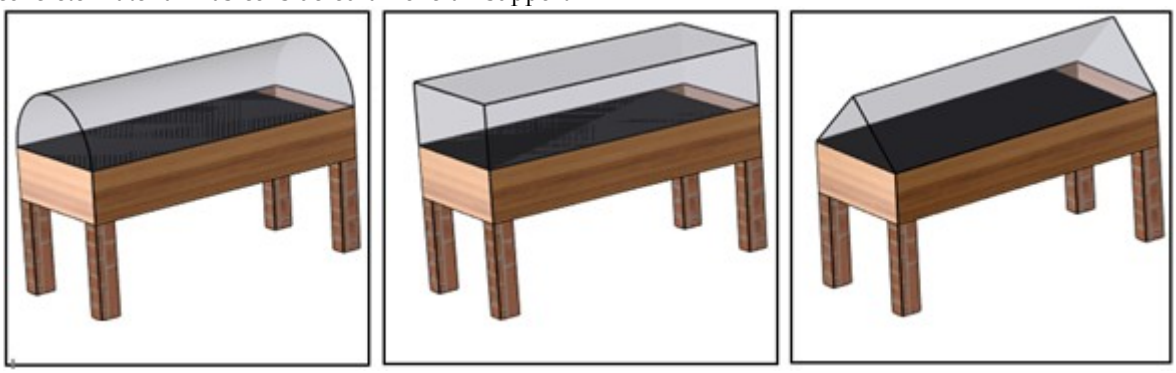

Figure 1. 3D Diagram of Semi-Circular (Quonset), Rectangular, and Triangular Shapes Respectively

The newly designed solar dryer is an active mode double air pass solar tunnel dryer with two main chambers. The heating chamber is the upper chamber, used to heat the incoming ambient air to enhance the thermal energy level of the air stream, and the drying chamber is the lower chamber, used to dry the product by transferring thermal energy stored in an air stream and concomitantly the air stream inside the chamber is heated for the second time by the back side of absorber plate. The ambient air enter and circulates inside the heating chamber. The hot air circulates inside the drying chamber. It exits from the chamber with a higher water vapor fraction with the help of the intake fan and ventilation fan, as indicated in the schematic diagram shown in Figure 2. A PV panel is mounted on the drying system to supply electrical energy for the fans.

Mathematical Modeling

A mathematical model was developed to obtain the outlet temperature of the air to assess the performance of a double air pass solar tunnel dryer.

Table 2. Design Specifications

Parameters	***Semi-Cylinder***	***Rectangular***	***Triangular***
Desired Collector Surface Area	$3.055\ m^2$	$3.055\ m^2$	$3.055\ m^2$
Collector Surface Area	$4.5\ m^2$	$4.364\ m^2$	$3.055\ m^2$
Face Surface Area	$0.3927\ m^2$	$0.5\ m^2$	$0.25\ m^2$
Floor Surface Area	$2.61\ m^2$	$1.9321\ m^2$	$1.9834\ m^2$
Absorber Plate Surface Area	$2.35\ m^2$	$1.74\ m^2$	$1.785\ m^2$
Width of Collector Surface	$1.571\ m$	$2\ m$	$1.4142\ m$
Length of Collector Surface	$2.61\ m$	$1.9321\ m$	$1.9834\ m$

Energy Balance of Glass Cover

The rate of thermal energy stored inside the cover material is the summation of the rate of solar energy absorbed by the cover, the rate of thermal energy exchange between the plate and cover through radiation, the rate of convective heat transfer between air stream inside a heating chamber and cover, the rate of radiative heat interaction between the sky and cover and the rate of thermal energy interaction with ambient through convection. The energy balance of the polyethylene cover is expressed as:

$$(m_c C_{pc})\left(\frac{dT_c}{dt}\right) = \begin{bmatrix} IA_c\alpha_c + A_p h_{pcr}(T_p - T_c) + A_c h_{acch}(T_{ah} - T_c) \\ -A_c h_{csr}(T_c - T_s) - A_c h_{camc}(T_c - T_{am}) \end{bmatrix} \quad (1)$$

Energy Balance on Absorber Plate

The rate of thermal energy accumulated in the absorber plate is equal to the summation of the rate of solar radiation absorbed by the plate, the rate of heat transfer between the plate and cover through convection, the rate of heat transfer between plate and floor through radiation, the rate of convective heat transfer between plate and air stream inside a heating chamber and the rate of convective heat transfer between plate and air stream inside the drying chamber. The energy balance of the absorber plate is expressed as:

$$(m_p C_{pp})\left(\frac{dT_p}{dt}\right) = \begin{bmatrix} IA_p\alpha_p\tau_c - A_p h_{pcr}(T_p - T_c) - A_p h_{pfr}(T_p - T_f) \\ -A_p h_{acch}(T_p - T_{ah}) - A_p h_{accd}(T_p - T_{ad}) \end{bmatrix} \quad (2)$$

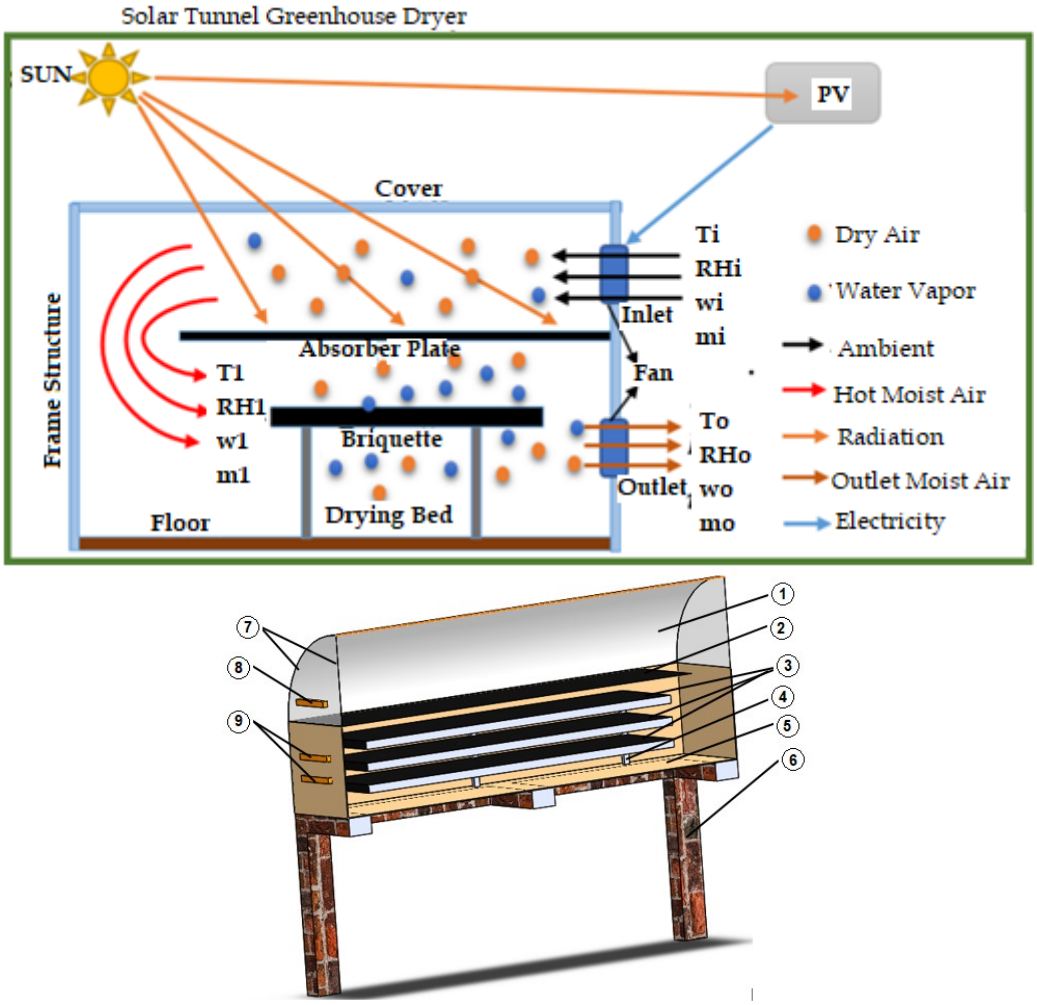

Figure 2. Schematic Diagram of the Proposed Drying System (1. Polyethylene Cover, 2. Absorber Plate, 3. Biomass Charcoal Briquette, 4. Drying Bed, 5. Bottom floor, 6. Overall Support Structure, 7. Frame Structure, 8. Air Inlet and 9. Air Outlet)

Energy Balance on Air Stream Inside Heating Chamber

The rate of thermal energy gained by the air stream is equal to the sum of the rate of solar radiation utilized by the air stream, the rate of convective heat transfer between plate and air stream inside the heating chamber, the rate of convective heat transfer between air stream inside a heating chamber and cover and the rate of thermal energy gain by air stream inside heating chamber due to the continuous air inflow and outflow. The energy balance of the air stream inside the heating chamber is expressed as:

$$\left(m_{ah}C_{pa}\right)\left(\frac{dT_{ah}}{dt}\right)=\begin{bmatrix} IA_c\alpha_a\tau_c+A_ph_{acch}\left(T_p-T_{ah}\right) \\ -A_ch_{acch}\left(T_{ah}-T_c\right)-\dot{m}_aC_{pa}\left(T_{ah}-T_{ai}\right)\end{bmatrix} \quad (3)$$

Where: $\alpha_a=\left[\left(1-F_p\right)\left(1-\alpha_p\right)+\left(1-\alpha_p\right)F_p\right]$

Energy Balance on Air Stream Inside Drying Chamber

The rate of thermal energy gain by the air stream inside the drying chamber is equal to the sum of the rate of convective heat transfer between the plate and air stream inside the drying chamber, the rate of convective heat transfer between the air stream inside the drying chamber and floor and the rate of thermal energy gain by air stream due to the continuous inflow and outflow of air inside drying chamber. The energy balance of the air stream inside the drying chamber is expressed as:

$$\left(m_{ad}C_{pa}\right)\left(\frac{dT_{ad}}{dt}\right)=A_ph_{accd}\left(T_p-T_{ad}\right)-A_fh_{accd}\left(T_{ad}-T_f\right)-\dot{m}_{ad}C_{pa}\left(T_{ad}-T_{ah}\right) \quad (4)$$

Energy Balance of the Bottom Floor

The rate of thermal energy accumulated on the bottom floor is the sum of the rate of radiative heat transfer between the absorber plate and the bottom floor, the rate of thermal energy exchange between the air stream inside the drying chamber and the bottom floor and the rate of thermal energy loss from the bottom floor to the ambient through convection.

$$\left(m_fC_{pf}\right)\left(\frac{dT_f}{dt}\right)=A_ph_{pfr}\left(T_p-T_f\right)+A_fh_{accd}\left(T_{ad}-T_f\right)-A_fU_b\left(T_f-T_{am}\right) \quad (5)$$

Energy and Exergy Analysis

Energy and exergy analyses are conducted to evaluate the amount of energy received, the effectiveness of energy utilization, and the capability of useful work extraction by the drying system. This

study investigated the selection of an effective solar tunnel dryer shape, the effect of air stream velocity variation, and the effect of input heat flux variation through energy and exergy analysis, also for the enhancement of energy utilization, energy conversion, and useful work extraction potential of the drying system for the increment of its performance. The energy and exergy value of the dryer is determined by applying steady-state analysis based on the initial and final state of air stream temperature at a given time (Castro et al., 2018;Panwar et al., 2013; Suherman et al., 2020).

Energy Analysis

Energy is the capacity to do work, and the analysis was performed based on the first law of thermodynamics. The incoming solar radiation is converted into useful thermal energy by increasing the energy level of the air stream and some amount of energy wasted due to optical loss, thermos-physical properties of dryer components, and temperature gradient between the air inside and outside of the dryer. Thus, the rate of solar energy input, useful energy utilized, thermal energy loss, and thermal efficiency of the drying system is computed based on mass and energy conservation principles. The Rate of Energy Input ($\dot{Q}_{in}$): computed as the product of the rate of incident solar radiation and the projected area of the drying system, expressed as:

$$\dot{Q}_{in} = A_{pr} I \tag{6}$$

The Rate of Useful Energy Output ($\dot{Q}_u$): evaluated as the difference between the output and input thermal energy state of the air stream, expressed as:

$$\dot{Q}_u = \dot{m}_a C_{pa}(T_{ao} - T_{ai}) \tag{7}$$

Thermal efficiency (η_{th}): of solar tunnel dryer is a measure of its performance toward conversion of incident solar radiation to useful thermal energy and is defined as the ratio of useful heat energy gained to the solar radiation input. Thus, the instantaneous thermal efficiency is given by:

$$\eta_{th} = \frac{\dot{Q}_u}{\dot{Q}_{in}} \tag{8a}$$

$$\eta_{th} = \frac{\dot{m}_a C_{pa}(T_{ao} - T_{ai})}{A_{pr} I} \tag{8b}$$

Exergy Analysis

Exergy is defined as the capability to extract valuable work, and the analysis was performed based on the second law of thermodynamics. The portion of energy converted to useful work is known as exergy output (available energy), and the rest that cannot be converted to work is exergy loss (unavailable energy). The property of exergy analysis is used to determine the quality of energy destruction and compare the useful work extraction potentials of the drying system. Therefore, the rate of exergy input, exergy output, exergy loss, and exergy efficiency of the drying system can be computed.

The Rate of Exergy Input ($\dot{E}x_{in}$): defined as a function of solar energy input, ambient temperature, and sun temperature, expressed as:

$$\dot{E}x_{in} = A_{pr} I \left[1 - \left(\frac{T_{am}}{T_{sun}}\right)\right] \tag{9}$$

The Rate of Exergy Output ($\dot{E}x_u$): computed as a function of the rate of useful energy output, air temperature at the inlet, and air temperature at the outlet, that can be computed by:

$$\dot{E}x_u = \dot{m}_a C_{pa}(T_{ao} - T_{ai})\left[1 - \left(\frac{T_{am}}{T_{ao}}\right)\right] \tag{10}$$

Exergy Efficiency (η_{ex}): is a measure of the useful work potential of the energy contained in a solar tunnel dryer at a specified state, defined as a ratio of the rate of useful exergy output to the rate of exergy input. Thus, the instantaneous exergy efficiency is expressed by:

$$\eta_{exh} = \frac{\dot{E}x_{uh}}{\dot{E}x_{in}} \tag{11a}$$

$$\eta_{exh} = \frac{\dot{m}_{ah} C_{pa}(T_{ah} - T_{ai})\left[1 - \left(\frac{T_{am}}{T_{ah}}\right)\right]}{A_{pr} I \left[1 - \left(\frac{T_{am}}{T_{sun}}\right)\right]} \tag{11b}$$

RESULTS AND DISCUSSION

The effect of ambient parameters on the drying system was investigated based on the weather condition of Jimma zone, Ethiopia. Inlet air temperature, the shape of STD, incident solar radiation over the projected area, and air stream velocity were taken as independent variables. In the analysis, the air stream temperature at the inlet of the heating chamber was similar to the ambient air temperature that varies concerning heat flux input variation over time, respectively, and the outlet air stream temperature of the heating chamber was considered as the inlet temperature of the drying chamber. The results obtained from mathematical model analysis were discussed in this section to identify the influence of heat flux input variation on outlet air stream temperature, energy, and exergy performance of the heating and drying chamber of the proposed drying system.

Outlet Air Temperature

Figure 3 shows the profiles of temperature variation at the outlet of the heating and drying chamber with heat flux input variation over time for three shapes by considering a constant air velocity $0.89\ m/s$. The air stream temperature ranges from $21°C$to $58.23°C$, $17.1°C$to$40.4°C$, and $20.22°C53.63°C$to at the outlet of the heating chamber. It varies from $22.4°C63.45°C18.24°C45.18°C21.46°C$and to $58.57°C$the outlet of the drying chamber for Quonset, rectangular and triangular shapes, respectively. A higher value of outlet temperature was found at a higher amount of heat flux input; when the amount of heat flux input reduces, the value of outlet temperature decreases for both chambers. Thus, the fluctuations of the heat flux input over time considerably affect the air stream temperature at the outlet of the heating and drying chamber (Karthikeya et al., 2017; Salvatierra-Rojas et al., 2021). Therefore, the value of air stream temperature at the outlet of both chambers was

affected by the value of ambient parameters but is highly affected by the amount of heat flux input, and a similar result was reported in the literature (Oueslati et al., 2018; Thakre et al., 2016).

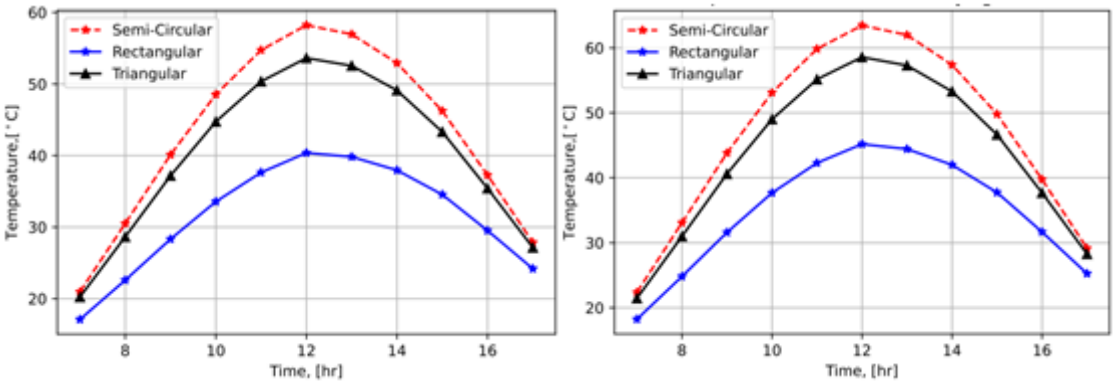

Figure 3. Outlet Air Temperature for each STD Shape, Heating and Drying Chamber.

The obtained result reveals that a higher temperature at the outlet of both chambers was found for the semi-circular (Quonset) shape than other shapes, followed by the triangular shape, and the slightest temperature is generated in the rectangular shape, shown in Fig. 3. Thus, at a constant air mass flow rate and heat flux input, a better amount of outlet temperature was found for the Quonset shape than other shapes. Therefore, the value of outlet temperature was affected by the STD shape change, and a similar result was reported in the literature (Jagadeesh et al., 2020; Khallaf et al., 2020; Missana et al., 2020; Perret et al., 2005; Vivekanandan et al., 2020).

Figure 4 shows the variation of outlet air temperature as a function of time for different air by considering Quonset shape STD and mass flow rate listed in Table 1. The obtained result from mathematical model simulation clearly shows that the air stream temperature ranges from 21°C to 58.3°C, 18.5°C to 46.4°C, 17.4°C to 40.8°C and 16.8°C to 37.4°Cat the outlet of the heating chamber and varies from 22.4°C to 63.65°C, 19.7°C to 51.8°C, 18.44°C to 45.7°C and 17.7°C to 41.7°Cat the outlet of the drying chamber with 0.8923, and 4 m/s air velocity, respectively. The higher air stream temperature at the outlet of both chambers was found for a lower air velocity of 0.89 $m/s$and the lower value was found for a higher air velocity of 4 m/s, the rest lies in between concerning each heat flux input. Figure 4 exhibits that in both chambers, the amount of outlet temperature decreases when air velocity increases due to an increase in air mass flow rate corresponding to air velocity input, which causes the reduction of air stream heating time. Thus, the change in air stream velocity affects the amount of outlet temperature generated, and a similar result was reported in the literature (Ekka et al., 2020; Ullah & Kang, 2017).

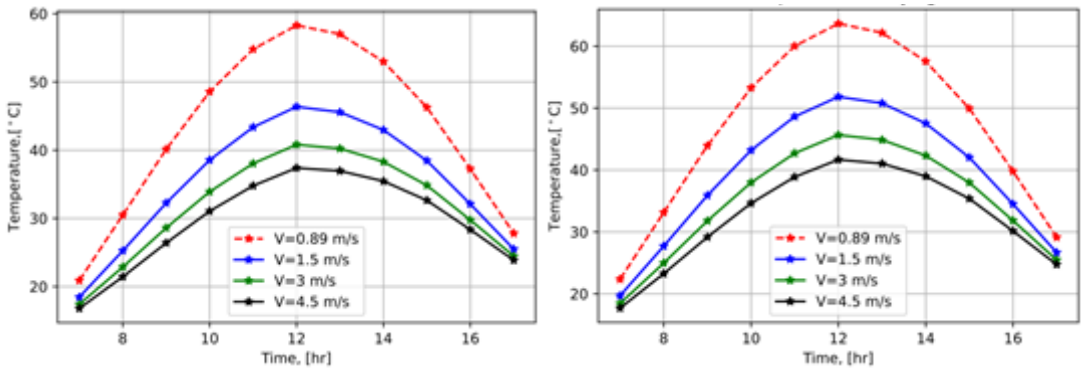

Figure 4. Outlet Air Temperature for Different Air Velocity.

Energy Performance

Figure 5 shows the variation of useful energy output as a function of drying time for variable heat flux input and three shapes. The useful energy output ranged from 115.45 W675.33 W45.24 W350.57 $W$and 102.24 W591.7 $W$to inside the heating chamber. It varied from 50.4 W to 184.65 W, 40.55 W to169.9 W43.62 W174.61 W,n of thermal efficiency as a function of drying time, which varied from 19.5 %to 21.4 %, 7.63 % to 10.94 %, and 17.25 % to 18.74 %in the heating chamber, and from 5.75 % to 8.5 %, 5.3 % to6.84 %, and 5.44 % to 7.36 % in the drying chamber for Quonset, rectangular and triangular shape STD, respectively. Compared to the heating chamber, the sound energy output and thermal efficiency of the drying chamber were lower

due to the higher inlet temperature (Pankaew et al., 2020). The result indicates that when the value of heat flux input increases, the amount of useful energy output increases, but the magnitude of thermal efficiency decreases. Therefore, the energy extraction performance of the proposed STD was affected by the amount of heat flux input, and a similar result was reported literature (Ayyappan et al., 2021; Rabha et al., 2017; Pankaew et al., 2020; Suherman et al., 2020).

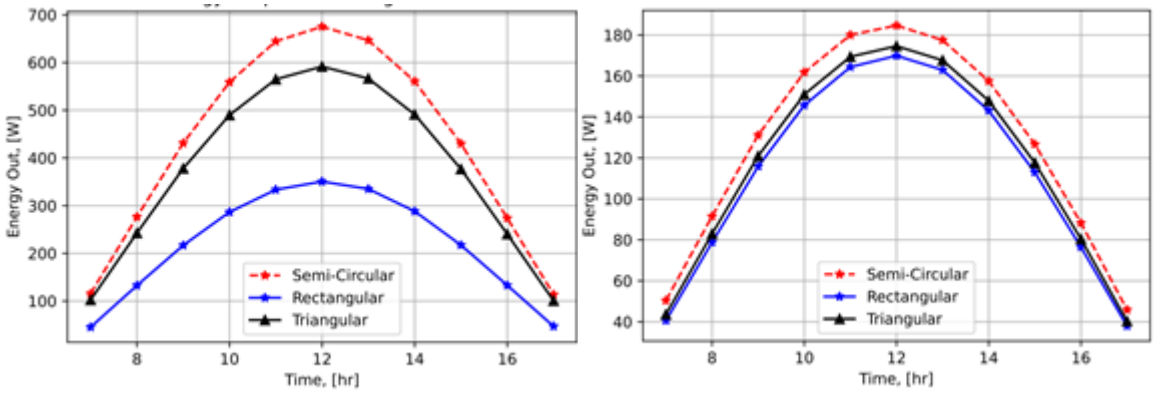

Figure 5. Useful Energy Output of Heating and Drying Chamber for each STD Shape.

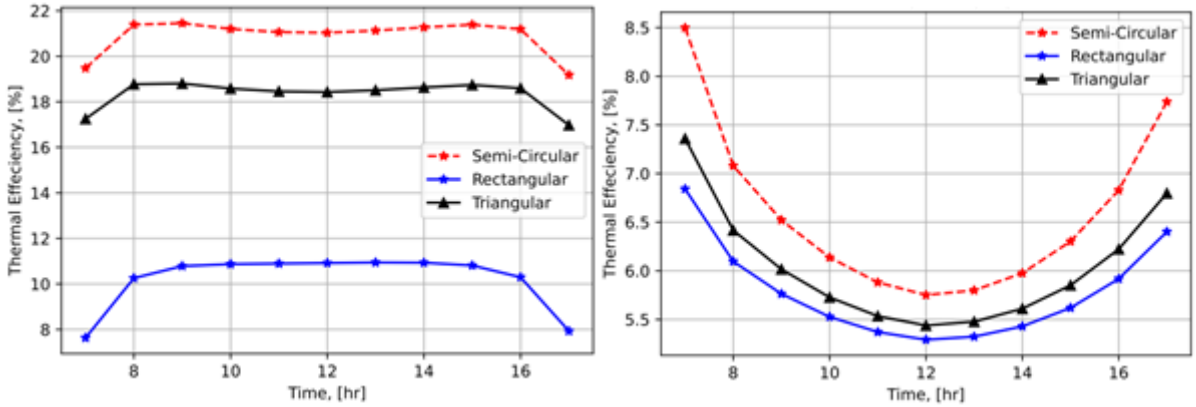

Figure 6. Thermal Efficiency of Heating and Drying Chamber for each STD Shape.

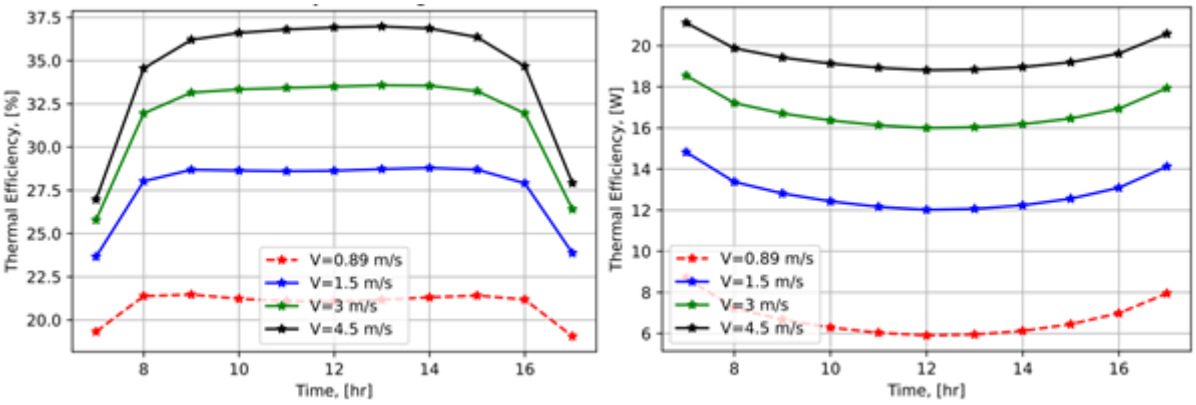

Figure 7. Useful Energy Output of Heating and Drying Chamber for each Air Velocity .

Figures 5 and 6 indicate that a higher amount of useful energy output and thermal efficiency was found for the Quonset shape due to its larger absorber plate area than other shapes, followed by the triangular shape, and the least value is generated in the rectangular shape at a constant mass flow rate. Thus, the better capacity of thermal energy extraction was found for the Quonset shape, followed by the triangular shape, and the least in the rectangular shape. Therefore, the energy extraction performance of the proposed STD was affected by the shape of the drying system, and a similar result was reported in the literature (Afshari et al., 2021; Ayyappan et al., 2021; Rabha et al., 2017; Pankaew et al., 2020; Suherman et al., 2020).

Figure 7 illustrates the profiles of thermal energy extraction efficiency variation over time with air velocity input in both chambers, and the value ranged from 19.05 % to 21.4 %, 23.66 % to 28.8 %, 25.78 % to33.6 %, and 27 % to 37 %for the heating

chamber and varied from 5.91 % to 8.7 %, 12.02 % to 14.82 %, 16 % to18.55 %, and 18.81 % to 21.11 %in the drying chamber for 0.89,23 and 4 m/s, respectively. The higher capacity of thermal efficiency generation was found when air velocity was higher, and the least capacity was observed when air velocity was lower. In both chambers, when the value of air velocity increases, the capacity of thermal efficiency generation increases concomitantly. Therefore, at a constant heat flux input and for a specific solar tunnel dryer geometry, the amount of useful energy extraction performance of the proposed STD was affected by the air velocity variation, and a similar result was reported in the literature (Afshari et al., 2021; Castro et al., 2018).

Exergy performance

Figure 8 shows the variation of useful exergy output as a function of drying time for variable heat flux input and three shapes. The useful exergy output varies from 10.85 W to 359.01 W, 1.01 W to60.72 W, and 4.1 W to 133.81 $W$for the heating chamber and ranges from 20.1 W to 588.41 W, 2.26 W to93.8 W, and 11.9 W to 351.43 W for the drying chamber. Figure 9 shows that the exergy efficiency ranged from 7.57 % to 13.78 %, 2.01 % to5.94 %, and 4.1 % to 7.14 % for the heating chamber, and ranges from 14.41 % to 22.6 %, 4.3 % to9.2 %, and 12.02 % to 18.75 % in Quonset, rectangular, and triangular shape STD, respectively. The fluctuation of useful exergy output and exergy efficiency is considerably influenced by heat flux input variation over time. Comparatively, the value of useful exergy output and exergy efficiency of the heating chamber was higher than the drying chamber due to higher air temperature at the inlet of the drying chamber. In both chambers, as the amount of heat flux input increases concomitantly, the capacity of useful work extraction and exergy efficiency also increases because of higher outlet temperature achievement at a higher heat flux (Ayyappan et al., 2021; Rabha et al., 2017; Pankaew et al., 2020; Suherman et al., 2020).

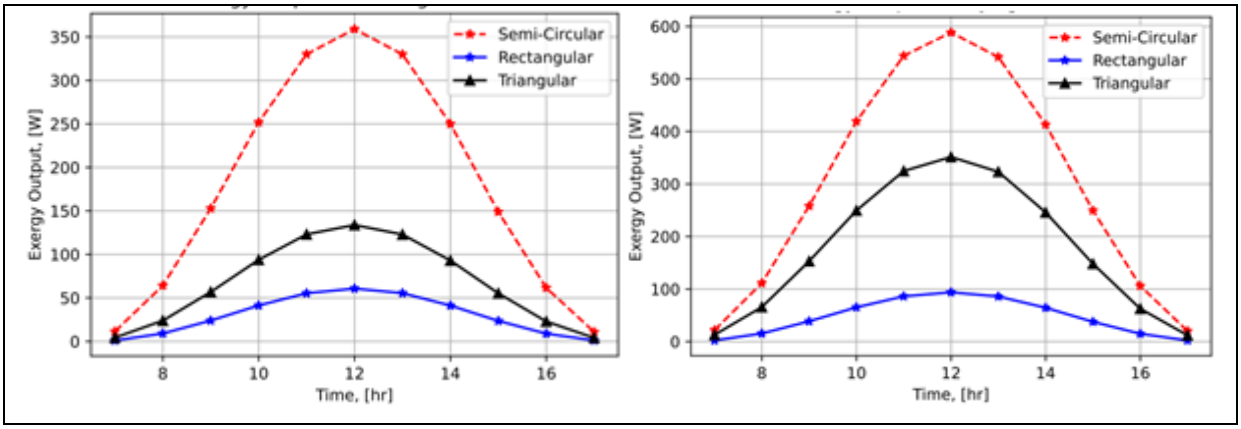

Figure 8. Useful Exergy Output of Heating and Drying Chamber for each STD Shape

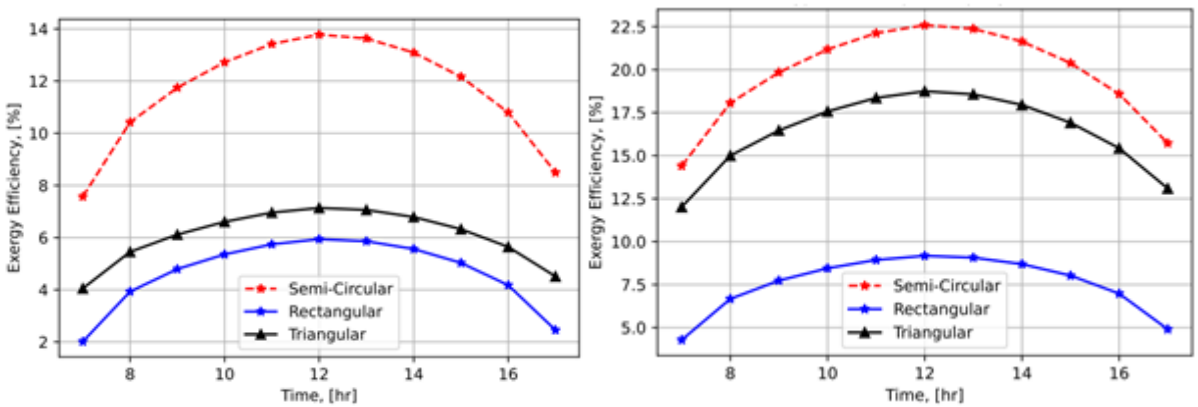

Figure 9. Exergy Efficiency of Heating and Drying Chamber for each STD Shape

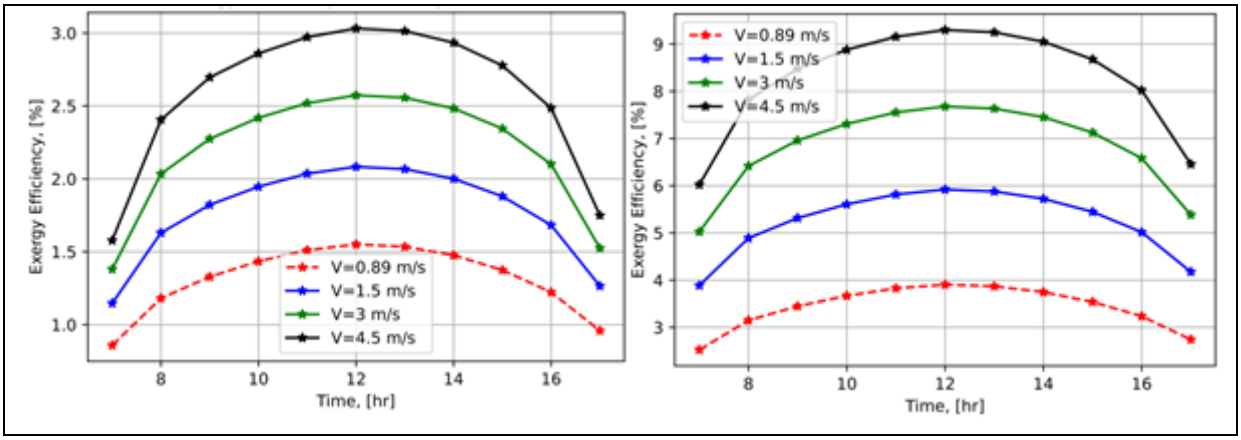

Figure 10. Thermal Efficiency of Heating and Drying Chamber for each Air Velocity.

The obtained analytical result reveals that in both chambers, the higher value of useful exergy output and exergy efficiency were observed for semi-circular (Quonset) STD shape than other shapes, followed by triangular shape, and the least value was found for a rectangular shape, shown in Figure 8 and Figure 9. Comparatively, at a constant mass flow rate, heat flux input, and collector surface area, STD with a semi-circular (Quonset) shape has a better exergy performance than other shapes, followed by a triangular and the least rectangular shape. The mathematical model simulation result of this study and the related study literature noticeably indicates that semi-circular (Quonset) shape STD has a better capacity for work extraction and exergy efficiency than rectangular and triangular shape STD (Afshari et al., 2021; Ayyappan et al., 2021; Rabha et al., 2017; Pankaew et al., 2020; Suherman et al., 2020).

Figure 10 shows the variation of exergy efficiency as a function of drying time for different velocities. The exergy efficiency ranges from 0.86 % to 1.55 %, 1.15 % to 2.1 %, 1.4 % to2.6 %, and 1.6 % to 3.03 %in the heating chamber and ranges from 2.52 % to 3.91 %, 3.89 % to 5.92 %, 5.03 % to7.68%, and 6.02 % to 9.3 %in the drying chamber, for 0.89, 23and 4 m/s, respectively. A higher capacity of work extraction and exergy efficiency in both chambers were found for a higher air velocity 4 m/sthan a lower one1 m/s. As the air velocity increases, the capacity of work extraction and exergy efficiency increases in both chambers. Therefore, air velocity variation affected the useful exergy output and exergy efficiency at a constant heat flux input and solar tunnel dryer geometry (Afshari et al., 2021; Castro et al., 2018).

CONCLUSION

This work investigated the design and analysis of an active mode double air pass solar tunnel dryer for drying charcoal dust briquette and evaluating its performance. The influence of solar tunnel dryer shape, heat flux input, and air velocity on outlet air temperature, energy, and exergy parameters was studied by developing a mathematical model. The numerical solution was obtained using a PYTHON code. The outlet temperature, thermal efficiency, and exergy efficiency vary from $21-58.23℃$, $19.5-21.4\%$and $7.6-21.2\%$, in the heating chamber and also vary from $22.4-63.45℃$, $5.75-8.5\%$and $14.41-22.6\%$, in the drying chamber, respectively, for heat flux input variation between 194 W/m^2 and 1052 W/m^2 at 0.89 m/s for a semi-circular shape dryer. The effect of the solar tunnel dryer shape was assessed. The higher outlet temperature, energy, and exergy value was found for a semi-circular shape, followed by a triangular shape. The most negligible value was found for a rectangular shape. The analysis of air velocity variation reveals that the value of energy and exergy efficiency increases, and outlet temperature decreases as air velocity increases. Therefore, the performance of an active mode double air pass solar tunnel dryer is affected by geometry (shape), input heat flux, and air stream velocity.

ACKNOWLEDGMENTS

The authors gratefully acknowledge Dire Dawa Institute of Technology and Jimma Institute of Technology for sponsoring the first author under the Ph.D. program. The authors are thankful to Sustainable Energy Engineering, Jimma Institute of Technology, for the opportunity to work on this study

REFERENCES

Afshari, F, Khanlari, A, Tuncer, AD and Sozen, A. 2021. Sahinkesen, I., Di-Nicola, G. Dehumidification of sewage sludge using Quonset solar tunnel dryer: An experimental and numerical approach. *Renewable Energy*. 171: 784-798.

Arisaka, J. 2019. Recycled charcoal briquettes in Mozambique - Affordable and quality energy for all. Verde Africa Ltd, Mozambique.

Ayyappan, SS, Selvakumar, M, Muthukannan, Karunaraja, N and Kumar, TR. 2021. Energy and Exergy Analyses of Coconut Drying in a Solar Tunnel Drier. *Process Mechanical Engineering*.

Castro, M, Román, C, Echegaray, M, Mazza, G and Rodriguez, R. 2018. Exergy Analyses of Onion Drying by Convection: Influence of Dryer Parameters on Performance. *Entropy. 20*: 310.

Ekka, JP, Bala, K, Muthukumar, P and Kanaujiya, D. K. 2020. Performance Analysis of a Forced Convection Mixed Mode Horizontal Solar Cabinet Dryer for Drying of Black Ginger

(KaempferiaParviflora) Using Two Successive Air Mass Flow Rates. *Renewable Energy*. 152: 55-66.

Guoa, Z, Wua, J, Zhang, Y, Wanga, F, Guoa, Y, Chena, K and Liu, H. 2020. Characteristics of biomass charcoal briquettes and pollutant emission reduction for sulfur and nitrogen during combustion. *Fuel*. 272: 117632.

Gupta, MK and Kaushik, SC. 2009. Performance Evaluation of Solar Air Heater for Various Artificial Roughness Geometries Based on Energy, Effective and Exergy Efficiencies. *Renewable Energy*. 34: 465-476.

Jagadeesh, D, Vivekanandan, M, Natarajan, A and Chandrasekar, S. 2020. Experimental Conditions to Identify the Ideal Shape of Dryer Investigation of Six Shapes of Solar Greenhouse Dryer in No Load. *Materials Today: Proceedings*.

Karthikeya, AK and Natarajan, R. 2017. Exergy Analysis and Mathematical Modelling of Orange Peels Drying in a Mixed Mode Solar Tunnel Dryer and Under the Open Sun: A Study On Performance Enhancement. *International Journal of Exergy*. 24 (2/3/4): 235-253.

Khallaf, AM, Tawfik, MA, El-Sebaii, AA and Sagaded, AA. 2020. Mathematical Modeling and Experimental Validation of the Thermal Performance of a Novel Design Solar Cooker. *Solar Energy*. 217: 40-50.

Kolesnikov, G and Gavrilov, T. 2020. Modeling the Drying of Capillary-Porous Materials in a Thin Layer: Application to the Estimation of Moisture Content in Thin-Walled Building Blocks. *Applied Sciences*. 10: 6953.

Missana, WP, Park, E and Kivevele, TT. 2020. Thermal Performance Analysis of Solar Dryer Integrated with Heat Energy Storage System and a Low-Cost Parabolic Solar Dish Concentrator for Food Preservation. *Journal of Energy*. 10: 9205283.

Mwampamba, TH, Owen, M and Pigaht, M. 2013. Opportunities, challenges, and the way forward for the charcoal briquette industry in Sub-Saharan Africa. *Energy for Sustainable Development*. 17: 158-170.

Ngusale, GK, Luo, Y and Kiplagat, JK. 2014. Briquette making in Kenya: Nairobi and peri-urban areas. *Renewable and Sustainable Energy Reviews*. 40: 749–759.

Oueslati, H, Mabrouk, SB and Mami, A. 2018. Thermal Modeling of Solar Dryer - Numerical Simulation, Analysis and Performance Evaluation. *International Journal of Air-Conditioning and Refrigeration*. 26 (4): 1850032.

Pankaew, P, Aumporn, O, Janjai, S, Pattarapanitchai, S, Sangsan, M and Bala, BK. 2020. Performance of a Large-Scale Greenhouse Solar Dryer Integrated with Phase Change Material Thermal Storage System for Drying of Chili. *International Journal of Green Energy*.

Panwar, NL, Kaushik, SC and Kothari, S. 2013. Thermal Modeling and Experimental Validation of Solar Tunnel Dryer: a Clean Energy Option for Drying Surgical Cotton. *International Journal of Low-Carbon Technologies*. 0: 1-13.

Perret, JS, Al-Ismaili, AM and Sablani, SS. 2005. Development of a humidification-Dehumidification System in a Quonset Greenhouse for Sustainable Crop Production in Arid Regions. *Biosystems Engineering*. 91 (3): 349-359.

Rabha, DK, Muthukumar, P and Somayaji, C. 2017. Energy and Exergy Analysis of the Solar Drying Processes of Ghost Chilli Pepper and Ginger. *Renewable Energy*. 105: 764-773.

Salvatierra-Rojas, A, Ramaj, I, Romuli, S and Müller, J. 2021. CFD-Simulink Modeling of the Inflatable Solar Dryer for Drying Paddy Rice. *Applied Science. 11*, 3118.

Suherman, S, Susanto, EE, Zardani, AW, Dewi, NHR and Hadiyanto, H. 2020. Energy–exergy analysis and mathematical modeling of cassava starch drying using a hybrid solar dryer. *Cogent Engineering*. 7 (1):1771819.

Thakre, PS, Deshmukh, SS and Jain, P. 2016. Design, Fabrication, and Performance Analysis of Solar Tunnel Dryer Using Various Absorber Materials. *International Advanced Research Journal in Science, Engineering, and Technology*. 3 (6): 2393-.

Ullah, F and Kang, M. 2017. Impact of Air Flow Rate on Drying of Apples and Performance Assessment of Parabolic Trough Solar Collector. *Applied Thermal Engineering*.

Vivekanandan, M, Periasamy, K, Dinesh Babu, C, Selvakumar, G and Arivazhagan, R. 2020. Experimental and CFD Investigation of Six Shapes of Solar Greenhouse Dryer in No Load Conditions to Identify the Shape of Dryer. *Materials Today: Proceedings*.